

# A mixed seismic-aseismic stress release episode in the Andean subduction zone

J. C. Villegas-Lanza<sup>1,2\*</sup>, J.-M. Nocquet<sup>2\*</sup>, F. Rolandone<sup>3</sup>, M. Vallée<sup>4</sup>, H. Tavera<sup>1</sup>, F. Bondoux<sup>5</sup>, T. Tran<sup>2†</sup>, X. Martin<sup>2</sup> and M. Chlieh<sup>2</sup>

**In subduction zones, stress is released by earthquakes and transient aseismic slip. The latter falls into two categories: slow slip and afterslip. Slow-slip events emerge spontaneously during the interseismic phase, and show a progressive acceleration of slip with a negligible contribution of synchronous tremors or microseismicity to the energy, or moment release<sup>1–12</sup>. In contrast, afterslip occurs immediately after large and moderate earthquakes, decelerates over time, and releases between 20 and 400% of the moment released by the preceding earthquake<sup>13–18</sup>. Here we use seismic and GPS data to identify transient aseismic slip that does not fit into either of these categories. We document a seismic-aseismic slip sequence which occurred at shallow depths along a weakly coupled part of the Andean subduction zone<sup>19</sup> in northern Peru and lasted seven months. The sequence generated several moderate earthquakes that together account for about 25% of the total moment released during the full sequence, equivalent to magnitude 6.7. Transient slip immediately followed two of the earthquakes, with slip slowing at a logarithmic rate. Considered separately, the moment released by transient slip following the second earthquake was more than 1,000% of the moment released during the earthquake itself, a value incompatible with classical models of afterslip. Synchronous seismic swarms and aseismic slip may therefore define a stress-release process that is distinct from slow-slip events and afterslip.**

Transient aseismic slip geodetically documented in subduction zones shows a great diversity of size, duration, temporal evolution of slip and seismic signature. Slow-slip events (SSE) lasting from weeks to months occur at depths of  $\sim 40$  km, downdip of the highly coupled portion of the subduction interface<sup>1–3</sup>. They often correlate with episodes of non-volcanic tremors (NVT; refs 3–5), contributing at most to 0.1% of the total moment released during the SSE (ref. 6). SSE detected in shallowly ( $< 20$  km) coupled subduction zones show durations of days to weeks<sup>7–11</sup>. They are usually associated with intense microseismicity bursts taking place inside or close to the slip area<sup>9–11</sup>, although non-volcanic tremors may also coexist<sup>12</sup>. In all cases of SSE documented so far, tremors and regular seismicity account for at most a few per cent (1–3%) of the total moment released<sup>6,9–11</sup>. Slow transient slip during days to months following moderate to large earthquakes, referred to as afterslip, has been extensively documented<sup>13–18</sup>. This process occurs in areas adjacent to the seismically ruptured zone<sup>18</sup> and its cumulative moment is usually 20–100% of the moment released by the earthquake<sup>3,17</sup>. Some cases

of unusually large afterslip (100–400% of the co-seismic moment) have also been reported following moderate to large earthquakes in the Japan<sup>13–15</sup> and Kamchatka<sup>16</sup> subduction zones. Thus, the aseismic/seismic moment ratio of processes releasing stress at subduction megathrust varies by four orders of magnitude, from  $10^{-1}$ – $10^0$  for earthquakes-afterslip sequences to  $10^2$ – $10^3$  for SSE, with a gap of processes with aseismic/seismic moment ratios of  $10^1$ .

Here, we use geodetic and seismological observations (Figs 1 and 2) to document a sequence mixing aseismic and seismic slip, both contributing significantly to the total moment release. The sequence took place in northern Peru, where the oceanic Nazca plate subducts predominantly aseismically beneath the Inca continental sliver at  $59 \text{ mm yr}^{-1}$  (ref. 19). Northern Peru had never experienced any great earthquake during the past five centuries, but hosted two significant earthquakes in 1960 ( $M_w$  7.6; ref. 20) and 1996 ( $M_w$  7.5; ref. 21). Both events were categorized as tsunami earthquakes because of their abnormally long source duration,

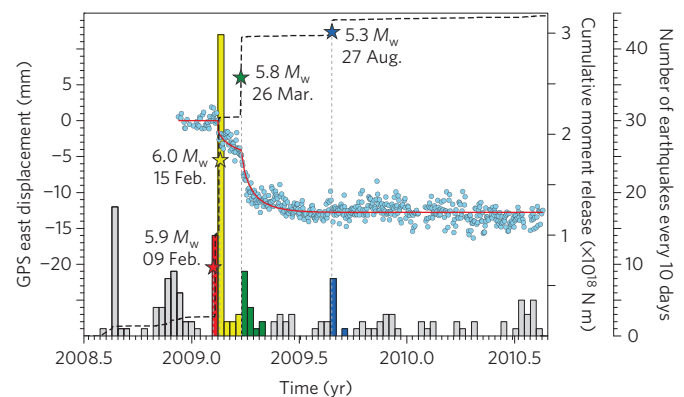


**Figure 1 | Geodetic time series and seismicity rate.** Blue dots indicate the east displacement recorded at GPS site BAYO expressed with respect to the overriding plate (left axis). Histogram bars show the number of seismic events in ten-day intervals (outside right axis). Histogram colours correspond to the time periods of Fig. 2. The stars show the dates of the four main earthquakes. Black dashed line represents the cumulated seismic moment through time (inside right axis). The red curve overprinting the GPS time series is the prediction from a simple spring-slider model with a velocity-strengthening friction law.

<sup>1</sup>Instituto Geofísico del Perú, Calle Badajoz 169, Urbanización Mayorazgo IV Etapa, Ate, 15012 Lima 03, Perú. <sup>2</sup>Geoazur, IRD, Université de Nice Sophia-Antipolis, Observatoire de la Côte d'Azur, CNRS, 250, rue A. Einstein, 06560 Valbonne, France. <sup>3</sup>Sorbonne Universités, UPMC Univ Paris 06, CNRS, Institut des Sciences de la Terre de Paris (ISTeP), 4, Place Jussieu, 75005 Paris, France. <sup>4</sup>Institut de Physique du globe de Paris, Sorbonne Paris Cité, Université Paris Diderot, UMR 7154 CNRS, 75238 Paris cedex 05, France. <sup>5</sup>Géosciences Environnement Toulouse, Université Paul Sabatier, IRD, CNRS, Observatoire Midi-Pyrénées, 31400 Toulouse, France. <sup>†</sup>Present address: National University of Civil Engineering, 55, Giai Phong Road, Hai Ba Trung District, Hanoi, Vietnam. \*e-mail: juanCarlos.villegas@igp.gob.pe; nocquet@geoazur.unice.fr

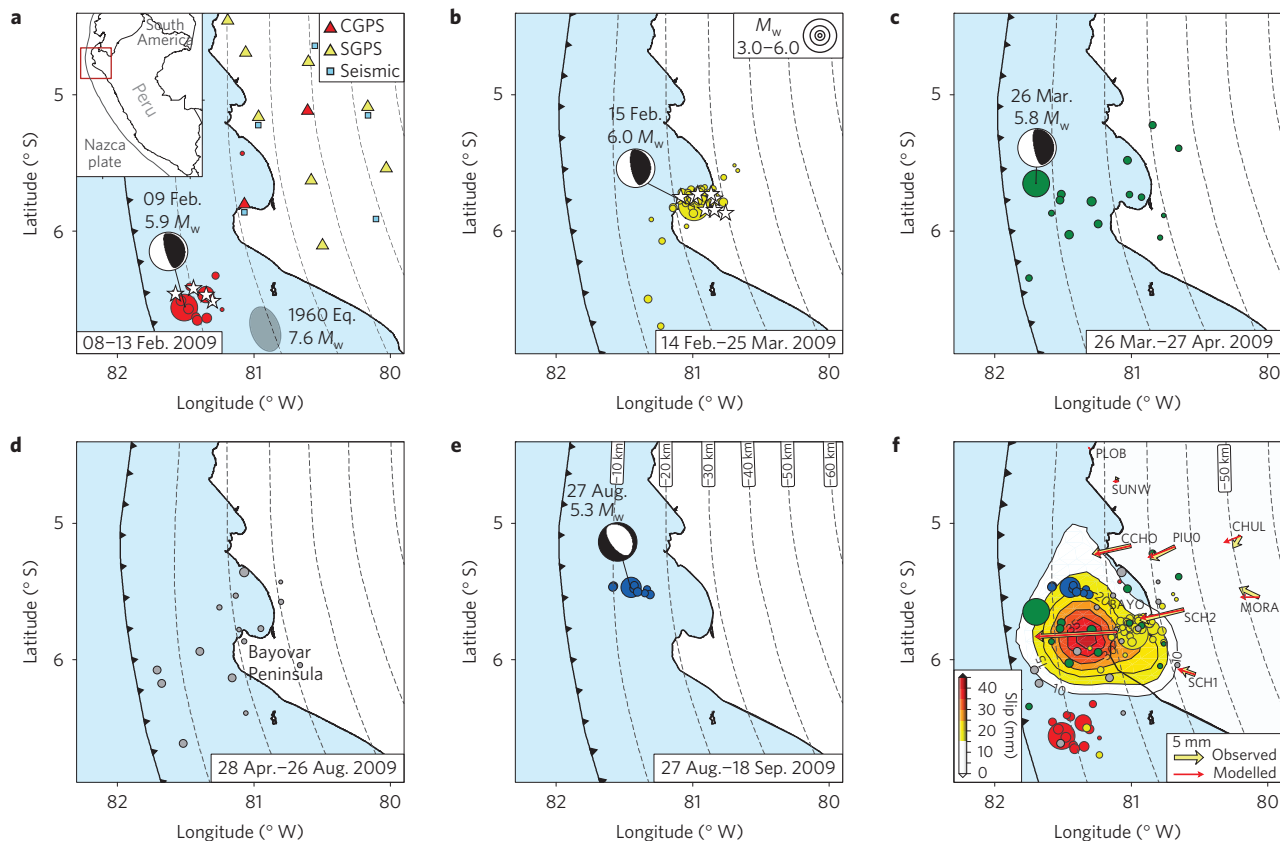


**Figure 2 | Time evolution of seismicity during the sequence and associated total slip. a–e,** Seismicity for five time windows. Circles scaled to magnitude show the location of earthquakes together with the focal mechanism and magnitude for the four largest events. The colour of circles indicates the time period as in Fig. 1. White stars are foreshocks. Light grey dashed lines are iso-depths of the subduction interface. The grey ellipse in **a** indicates the rupture area for the 1960  $M_w$  7.6 tsunami earthquake<sup>20</sup>. Red and yellow triangles indicate the location of continuous and survey GPS sites, respectively. Blue squares indicate the location of seismic stations. **f,** Slip distribution of the total cumulative displacement. Colours represent slip in mm and lines indicate isovalues of slip every 5 mm. Yellow and red arrows are the observed and modelled GPS displacements, respectively.

enhanced long-period source spectrum, and the relatively large induced tsunami, with run-up heights exceeding 5 m for the 1996 (ref. 21) and 9 m for the 1960 event<sup>20</sup>.

The 2009 sequence studied here occurred north of the rupture of the 1960 tsunami earthquake, possibly overlapping with it. A transient trenchward displacement is seen at the continuous GPS site BAYO, lasting seven months from February to September 2009, with a cumulative westward displacement of 14 mm (Fig. 1). Inversion of the slip distribution using geodetic displacements at 11 sites indicates that the main area of slip took place at shallow depth (<25 km) along the subduction interface, involving a patch of 90 km in diameter (Fig. 2f). The maximum slip reaches 45–50 mm and the equivalent moment release is  $M_w$  6.7–6.8. Between February and September 2009, the seismicity recorded by both the National Seismic Network of Peru and a temporary broadband seismometer network shows a sharp increase, with more than one hundred events with magnitude ranging from 2.9 to 6.0, all located inside or close to the slip area. The moment released through earthquakes is equivalent to  $M_w$  6.3, indicating that the process was ~70–85% aseismic.

The GPS time series at BAYO (Fig. 1) further shows that the slip evolved through time, with phases of acceleration, which correlate with the occurrence of the major earthquakes, before a final phase of deceleration that lasted five months (Fig. 1). The recorded seismicity also shows a spatial and temporal organization related to the occurrence of the major events, followed by a five-month period of relative quiescence (Fig. 2). In the following, we describe the different phases of the sequence (Fig. 3) and discuss their

implications on the triggering process and the frictional anatomy of the plate interface. Our interpretation is illustrated in Fig. 4.

Before the sequence, interseismic GPS velocities indicate that the plate interface is predominantly creeping<sup>19</sup>, therefore implying a dominant velocity-strengthening friction regime. The Bayovar area shows regular moderate seismicity, with ~20 interface events in the magnitude range  $M_w$  5.1–6.0 recorded since 1976 (ref. 22). The occurrence of moderate interface earthquakes indicates the existence of locked velocity-weakening patches with typical sizes of 0.1 to 10 km, but still too small and too sparse to induce significant strain rate detectable by GPS during the interseismic period (Fig. 4a,b).

The sequence studied here started at a depth of ~12 km, ~30 km east from the trench. On 8 February 2009, a series of four foreshocks ( $M_w$  3.9 to 4.9) preceded, by 20 h to 30 min, a  $M_w$  5.9 thrust interface earthquake that occurred on 9 February. Eight aftershocks ( $M_w$  3.1 to 4.2) were detected in the two days following the main shock (Figs 2a and 4c). Because the seismic subsequence took place about ~100 km from the Peruvian coast, we could not observe whether it was associated with some aseismic slip or not.

The second subsequence started three days later, at ~20–25 km depth, ~100 km northeast of the first subsequence (Figs 2b and 4d) with eight foreshocks ( $M_w$  3.2 to 4.6) preceding, by 30 h to 10 min, an interplate earthquake ( $M_w$  6.0) on 15 February. Thirty-eight aftershocks with  $M_w$  2.9–4.2 occurred during the following five weeks. For both February events, the aftershocks are spatially clustered close to the epicentre, and occurred within a few days following the main shock, as commonly observed for  $M_w$  ~5.9–6.0

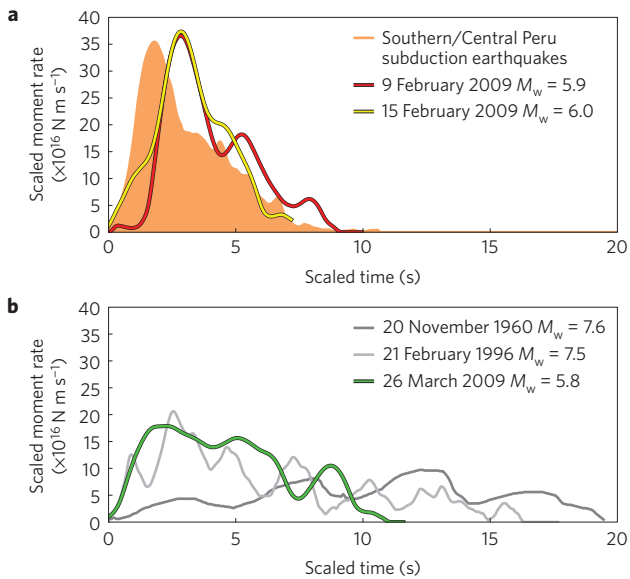


**Figure 3 | Comparison of normalized source time functions (NSTF).** The reference moment for normalization is  $M_w$  6.0. **a**, NSTF for the earthquakes of 9 and 15 February together with the average NSTF for central and southern Peru subduction earthquakes. **b**, NSTF for the 26 March earthquake, together with the NSTF for the 1960  $M_w$  7.6 (ref. 20) and 1996  $M_w$  7.5 (ref. 21) tsunami earthquakes. NSTF shown in **b** have a peak moment rate half or less of that of the average NSTF for Peru earthquakes, and have significantly longer durations.

earthquakes. Also, for both events, no clear transient signal is seen in the GPS time series before the main shock, indicating that if transient aseismic slip existed, it was small. By contrast, a transient slip is evidenced by the GPS time series at BAYO after the 15 February earthquake, with a trenchward displacement of  $\sim 4$  mm during the next 39 days (Fig. 1). Because transient slip for this period is not detected at the other CGPS site PIU0 (Supplementary Fig. 2), the transient signal seen at BAYO probably reflects some afterslip occurring in the immediate vicinity of the 15 February earthquake (Fig. 4d).

The next event (26 March  $M_w$  5.8) occurred at very shallow ( $\sim 8$  km) depth, close to the trench. Its characteristics depart from the two previous events, with neither foreshocks nor a clear sequence of spatially and timely clustered aftershocks (Fig. 2c). The seismicity in the following five months occurred over a wide area, at a rate not significantly different from the background seismicity before the sequence (Fig. 2c,d). We further find that the 26 March earthquake had a moment release duration of 9–10 s (for a magnitude  $M_w$  of 5.8), to be compared with the 5 s duration observed for the  $M_w$  6.0 15 February event. When normalized to an equivalent  $M_w$  6.0 earthquake<sup>23</sup>, the source time functions (STF) for the 9 February and 15 February are similar in shape and duration to the average STF derived for the subduction earthquakes that occurred in the highly coupled subduction segment in central and southern Peru (Fig. 3a). In contrast, the normalized STF for the 26 March earthquake shows a fairly long duration and low moment rate release throughout the rupture, two characteristics also shared by the 1960  $M_w$  7.6 and 1996  $M_w$  7.5 tsunami earthquakes<sup>20,21</sup> (Fig. 3b). The 26 March therefore probably occurred within the weak, low-rigidity material within the accretionary prism (Fig. 4e), which promotes a conditionally stable regime<sup>24</sup> where slip is generally stable and aseismic, but can be seismic if it experiences significant rapid loading<sup>23</sup>.

The rate and amount of aseismic slip drastically increased after the 26 March event, and was also detected at CGPS site PIU0,

$\sim 80$  km northeast from BAYO (Fig. 1 and Supplementary Fig. 2). The post-26 March earthquake transient displacement represents  $\sim 70\%$  of the cumulated displacement observed at site BAYO, despite a moment half that of the 15 February event and a more remote location from GPS site BAYO. Finally, a crustal  $M_w$  5.3 earthquake on 27 August marks the end of the sequence (Figs 1 and 2e). Its normal focal mechanism indicates that the stress previously released was large enough to reactivate a normal fault within the upper plate.

The logarithmic-like displacement seen in the BAYO GPS time series is similar to the post-seismic deformation observed after many earthquakes<sup>13–18</sup>, but with an unusually large aseismic/seismic moment ratio for the  $M_w$  5.8 26 March tsunami-type earthquake. Indeed, considered separately, the aseismic/seismic ratio for this event is  $>1,000\%$ . Such a ratio falls between those found for classical earthquake-afterslip sequences and for SSE, and has been previously observed only in the case of the 1992 Sanriku-Oki ultra-slow earthquake<sup>25</sup>.

Afterslip is commonly interpreted within the rate-and-state friction law framework<sup>24</sup> as the response of velocity-strengthening areas nearby the rupture to the sudden stress increment induced by the earthquake. The stress increment leads to an instantaneous increase of the sliding velocity in the nearby velocity-strengthening areas, which then decreases through time as logarithmic decay<sup>26</sup>. In Fig. 1, we show the transient displacement predicted by a simple spring-slider model with a velocity-strengthening law superimposed on the BAYO GPS time series (Supplementary Information). Although a good fit to the GPS time series is achieved by this model, it leads to some unrealistic physical parameters: because the stress increment induced by the co-seismic slip scales as the logarithm of the velocity increment, the 26 March earthquake should have generated a Coulomb stress increment at least five times larger than that of the 15 February earthquake, despite a two times smaller moment; because no significant co-seismic offset was detected at GPS site BAYO after the 26 March earthquake, we can exclude the 26 March earthquake having had an abnormally large slip (Supplementary Information). Furthermore, within the simple model of velocity-strengthening response to a sudden stress increment, the amount of triggered afterslip scales with the Coulomb stress change induced by the earthquake divided by the equivalent stiffness of the medium where afterslip occurs<sup>26</sup>. Previous large afterslip cases<sup>14,15</sup> are consistent with this view. Here, the Coulomb stress increment within the slip area is found to be of the order of a few kPa at most, unlikely to be able to produce the centimetres of slip observed here (Supplementary Information). A stress perturbation of a few kPa is a typical value that has been proposed for triggering or modulating SSE and NVT (refs 27–29). Together with the absence of seismicity following the 26 March earthquake, this correlation favours the view that the post-26 March aseismic slip was a slow slip ‘helped’ by an earthquake rather than classical afterslip. Results of the slip inversion suggest that part of the aseismic slip took place in the conditionally stable area close to the 26 March earthquake (Fig. 4e). To cause such a significant aseismic fault slip, this area should have accumulated observationally negligible, but still significant, elastic strain before the sequence (Fig. 4b). Possibly, the small seismic asperities (source regions of the 9 and 15 February, and 26 March earthquakes) might pin the plate interface during the interseismic phase so that the area between them can accumulate some elastic strain.

Seismic swarms (SS) are commonly observed along megathrust subduction zones<sup>30</sup>. Although the relationship of SS to aseismic slip has been proposed, very few observations have actually constrained the size and time evolution of the associated aseismic slip. The northern Peru 2009 sequence shows how different areas of the subduction interface can interact through time and space at distances several times larger than the size involved in individual subsequences (Figs 2 and 4). The mixed seismic

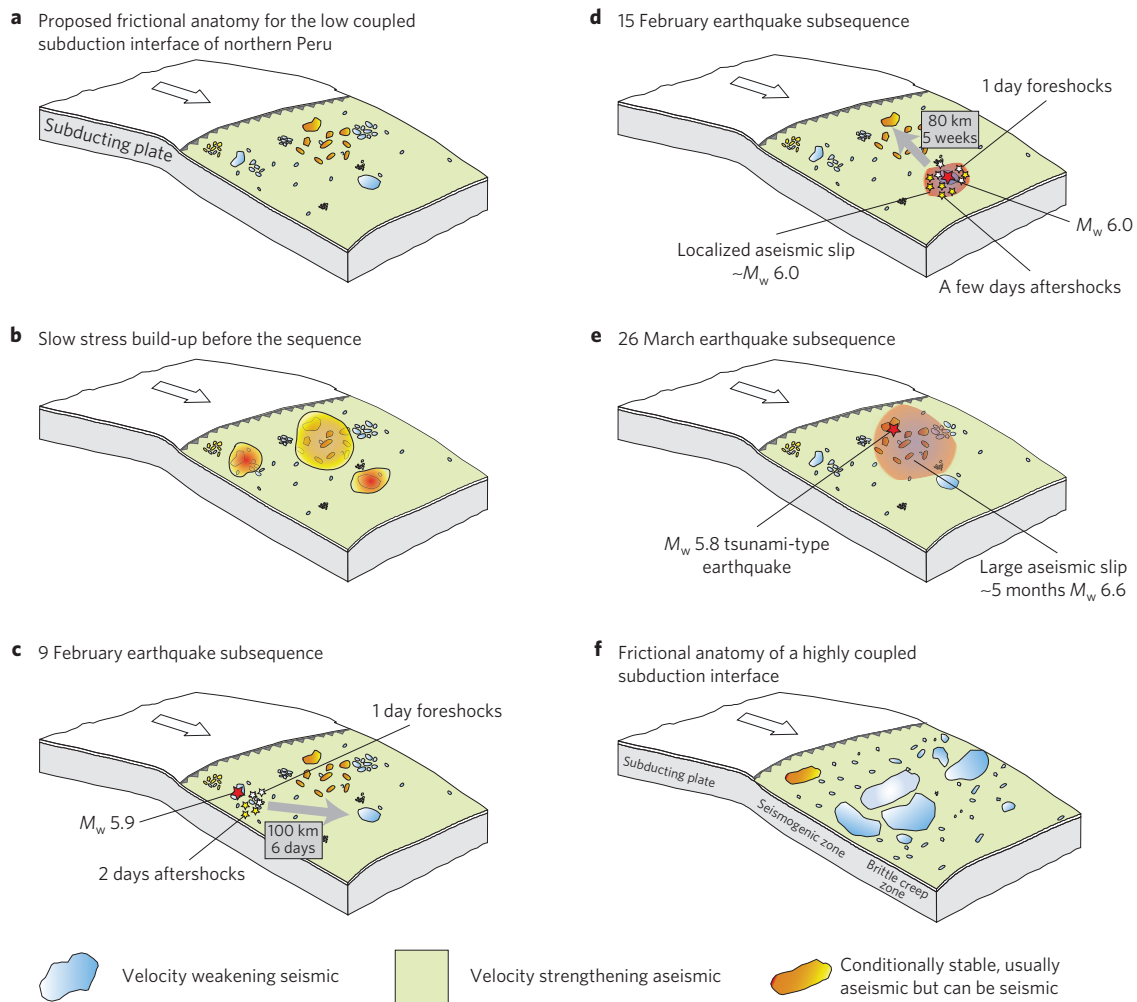


**Figure 4 | Conceptual model of the 2009 northern Peru sequence.** **a**, Proposed frictional anatomy for the low coupled subduction interface of northern Peru. **b**, Stress accumulation before the sequence. **c–e**, Foreshocks, mainshock and aseismic slip for the 9 February, 15 February and 26 March subsequences respectively. Grey arrows indicate the distance and time separation between a given sequence and the next one. **f**, For comparison, frictional anatomy for a highly coupled subduction interface.

and aseismic behaviours observed during the sequence witness the spatially variable frictional properties of a weakly coupled subduction interface. Although seismicity and NVT triggered by SSE and aseismic slip triggered by earthquakes had been recognized separately, we show that more complex interactions can exist between the two modes of slip. In that sense, the 2009 northern Peru sequence suggests that synchronous slow slip and seismic swarms at subduction megathrusts define a specific category of stress-release process.

## Methods

Methods and any associated references are available in the [online version of the paper](#).

Received 2 July 2015; accepted 18 November 2015;  
published online 21 December 2015

## References

- Ozawa, S., Murakami, M. & Tada, T. Time-dependent inversion study of the slow thrust event in the Nankai trough subduction zone, southwestern Japan. *J. Geophys. Res.* **106**, 787–802 (2001).
- Dragert, H., Wang, K. & James, T. S. A silent slip event on the deeper Cascadia subduction interface. *Science* **292**, 1525–1528 (2001).
- Schwartz, S. Y. & Rokosky, J. M. Slow slip events and seismic tremor at Circum-Pacific subduction zones. *Rev. Geophys.* **45**, 1–32 (2007).
- Rogers, G. & Dragert, H. Episodic tremor and slip on the Cascadia subduction zone: The chatter of silent slip. *Science* **300**, 1942–1943 (2003).
- Hirose, H. & Obara, K. Repeating short- and long-term slow slip events with deep tremor activity around the Bungo Channel region, southwest Japan. *Earth Planets Space* **57**, 961–972 (2005).
- Kao, H., Wang, K., Dragert, H., Kao, J. Y. & Rogers, G. Estimating seismic moment magnitude ( $M_w$ ) of tremor bursts in northern Cascadia: Implications for the ‘seismic efficiency’ of episodic tremor and slip. *Geophys. Res. Lett.* **37**, L19306 (2010).
- Wallace, L. M. & Beavan, J. Diverse slow slip behavior at the Hikurangi subduction margin, New Zealand. *J. Geophys. Res.* **115**, B12402 (2010).
- Douglas, A., Beavan, J., Wallace, L. & Townend, J. Slow slip on the northern Hikurangi subduction interface, New Zealand. *Geophys. Res. Lett.* **32**, L16305 (2005).
- Delahaye, E. J., Townend, J., Reyners, M. E. & Rogers, G. Microseismicity but no tremor accompanying slow slip in the Hikurangi subduction zone, New Zealand. *Earth Planet. Sci. Lett.* **277**, 21–28 (2009).
- Ozawa, S., Suito, H. & Tobita, M. Occurrence of quasi-periodic slow-slip off the east coast of the Boso Peninsula, Central Japan. *Earth Planets Space* **59**, 1241–1245 (2007).
- Vallée, M. *et al.* Intense interface seismicity triggered by a shallow slow slip event in the Central Ecuador subduction zone. *J. Geophys. Res.* **118**, 2965–2981 (2013).
- Walter, J. I., Schwartz, S. Y., Protti, J. M. & Gonzalez, V. Persistent tremor within the northern Costa Rica seismogenic zone. *Geophys. Res. Lett.* **38**, L01307 (2011).
- Heki, K., Miyazaki, S. & Tsuji, H. Silent fault slip following an interplate thrust earthquake at the Japan Trench. *Nature* **386**, 595–598 (1997).

14. Yagi, Y., Kikuchi, M. & Sagiya, T. Co-seismic slip, post-seismic slip, and aftershocks associated with two large earthquakes in 1996 in Hyuga-nada, Japan. *Earth Planets Space* **53**, 793–803 (2001).
15. Suito, H., Nishimura, T., Tobita, M., Imakiire, T. & Ozawa, S. Interplate fault slip along the Japan Trench before the occurrence of the 2011 off the Pacific coast of Tohoku earthquake as inferred from GPS data. *Earth Planets Space* **63**, 615–619 (2011).
16. Bürgmann, R. *et al.* Rapid aseismic moment release following the 5 December, 1997 Kronotsky, Kamchatka, earthquake. *Geophys. Res. Lett.* **28**, 1331–1334 (2001).
17. Pritchard, M. E. & Simons, M. An aseismic slip pulse in northern Chile and along-strike variations in seismogenic behavior. *J. Geophys. Res.* **111**, B8405 (2006).
18. Perfettini, H. *et al.* Seismic and aseismic slip on the Central Peru megathrust. *Nature* **465**, 78–81 (2010).
19. Nocquet, J.-M. *et al.* Motion of continental slivers and creeping subduction in the northern Andes. *Nature Geosci.* **7**, 287–291 (2014).
20. Pelayo, A. M. & Wiens, D. A. The November 20, 1960 Peru tsunami earthquake: Source mechanism of a slow event. *Geophys. Res. Lett.* **17**, 661–664 (1990).
21. Ihmlé, P. F., Gomez, J.-M., Heinrich, P. & Guibourg, S. The 1996 Peru tsunamigenic earthquake: Broadband source process. *Geophys. Res. Lett.* **25**, 2691–2694 (1998).
22. Ekström, G., Nettles, M. & Dziewonski, A. M. The global CMT project 2004–2010: Centroid-moment tensors for 13,017 earthquakes. *Phys. Earth Planet. Inter.* **201**, 1–9 (2012).
23. Bilek, S. L. & Lay, T. Tsunami earthquakes possibly widespread manifestations of frictional conditional stability. *Geophys. Res. Lett.* **29**, 181–184 (2002).
24. Dieterich, J. H. Modeling of rock friction experimental results and constitutive equations. *J. Geophys. Res.* **84**, 2161–2168 (1979).
25. Kawasaki, I. *et al.* The 1992 Sanriku-Okii, Japan, ultra-slow earthquake. *J. Phys. Earth* 105–116 (1995).
26. Perfettini, H. & Avouac, J. Postseismic relaxation driven by brittle creep: A possible mechanism to reconcile geodetic measurements and the decay rate of aftershocks, application to the Chi-Chi earthquake, Taiwan. *J. Geophys. Res.* **109**, B02304 (2004).
27. Hawthorne, J. C. & Rubin, A. M. Tidal modulation of slow slip in Cascadia. *J. Geophys. Res.* **115**, B09406 (2010).
28. Ozawa, S. Shortening of recurrence interval of Boso slow slip events in Japan. *Geophys. Res. Lett.* **41**, 2762–2768 (2014).
29. Nadeau, R. M. & Guilhem, A. Nonvolcanic tremor evolution and the San Simeon and Parkfield, California, earthquakes. *Science* **325**, 191–193 (2009).
30. Holtkamp, S. G. & Brudzinski, M. R. Earthquake swarms in circum-Pacific subduction zones. *Earth Planet. Sci. Lett.* **305**, 215–225 (2011).

### Acknowledgements

This work has been funded by the ANR (Agence Nationale de la Recherche, contract number ANR-07-BLAN-0143-01) and has continuously been supported by the IRD (Institut de Recherche pour le Développement). We thank J. P. Ampuero from Caltech for the use of broadband seismic data from a temporary network in the frame of the Sisnort-08 project. J.C.V.-L. acknowledges support provided by the IRD-DSF through a PhD grant.

### Author contributions

J.C.V.-L. and J.-M.N. carried out fieldwork, GPS analysis and slip inversion; J.C.V.-L. performed the seismicity analysis; J.-M.N. and F.R. performed the rate-and-state calculations; M.V. conducted the source time functions analysis; M.C., F.B. and X.M. carried out GPS fieldwork; H.T. provided seismological data; T.T. performed GPS analysis; J.-M.N., F.R. and J.C.V.-L. wrote the paper. All authors discussed the results and commented on the manuscript.

### Additional information

Supplementary information is available in the [online version of the paper](#). Reprints and permissions information is available online at [www.nature.com/reprints](http://www.nature.com/reprints). Correspondence and requests for materials should be addressed to J.C.V.-L. or J.-M.N.

### Competing financial interests

The authors declare no competing financial interests.

## Methods

The GPS data are available on request to the corresponding authors. The seismological data are from the Geophysical Institute of Peru (IGP) and are subject to the agreement of IGP (contact: hernando.tavera@igp.gob.pe). GPS analysis and slip inversion codes are available on request from JMN.

**GPS.** We analyse the GPS data using the GAMIT/GLOBK 10.50 software<sup>31</sup> to derive daily estimates of GPS site positions. To improve the precision of our time series over the studied area, we define a local reference frame using six continuous GPS sites surrounding northern Peru that is then used to express our time series. We derive the displacements at 11 GPS and associated uncertainties (Supplementary Fig. 1 and Supplementary Table 1) using least squares and by simultaneously fitting a position at a reference epoch, a velocity and an offset on the horizontal components.

**Inversion.** We invert the slip distribution along the plate interface using the GPS displacements as input data. We discretize a 250-km-long segment of the subduction interface with 533 triangular subfaults from the trench to a depth of 60 km using a geometry modified from ref. 32. We calculate the Green's function relating the unit slip for a fixed rake of 90° of each subfault to the displacement components at the GPS sites for a homogeneous elastic semi-infinite space<sup>33</sup>. We use a least-squares inversion with regularization constraints<sup>34</sup> to retrieve the slip, and perform a resolution analysis of the inversion results<sup>35</sup>. Our results show that the downdip limit of the slip distribution is well constrained by the data and that 75 to 90% of the moment was released at depths shallower than 20 km, the deeper slip distribution being in the vicinity of the  $M_w$  6.0 15 February earthquake. The area of significant slip involves a 80-km-long segment of the subduction. The uncertainty for the slip amount and the slip spatial distribution increases with the distance from the coast. As a consequence, the western extent of the main slip patch is not resolved, and a larger slip than shown in Fig. 2f might have occurred close to the location of the 26 March earthquake. We find that the range of the total moment is conservatively in the range  $1.11\text{--}1.83 \times 10^{19}$  N m, with a preferred value of  $1.20 \times 10^{19}$  N m, equivalent to  $M_w$  6.7. Figure 2f shows a model derived using minimum Laplacian smoothing constraints and is selected using an L-curve criterion. The weighted root mean square (wrms) for this model is 1.0 mm.

**Seismicity.** We use five stations of the National Seismic Network of the Geophysical Institute of Peru and eight stations from a temporal local seismic network to analyse the seismicity for the period mid-2008 to mid-2010. We select 223 events (among them 102 belong to the 2009 sequence) with a minimum of four P- and S-arrival times. We estimate the detection level to be  $M_L \sim 3.2$ . We simultaneously derive a new one-dimensional velocity model and hypocentre location, using the Velest program<sup>36</sup>. The estimated depths agree within a few kilometres with our subduction interface geometry. We compute local magnitudes  $M_L$ , which we convert into  $M_w$  (see Supplementary Information) to evaluate the seismic moment released through earthquakes.

**Source time functions.** Source time functions (STFs) are extracted from the teleseismic P body waves recorded at the stations of the Federation of the Digital

Seismograph Networks (FDSN). For each earthquake, we use the SCARDEC method<sup>37</sup> to retrieve the apparent STFs at each station, from which we compute the average STF. The duration of the main moment release is evaluated from the average STF, between the first and last point reaching  $0.25F_m$ , where  $F_m$  is the peak of the moment rate. Because earthquake scaling laws predict that the STF duration and amplitude evolve as  $M_0^{1/3}$  and  $M_0^{2/3}$ , respectively<sup>23</sup> (where  $M_0$  is the seismic moment), we normalize the average STF (hereafter referred as NSTF) to a common seismic moment, here chosen equal to  $M_0^{\text{ref}} = 1.16 \times 10^{18}$  N m ( $M_w = 6.0$ ) to produce Fig. 3. For comparison, we compute the average NSTF of earthquakes for ten interplate earthquakes in the nearby central and southern Peru subduction zone with depths between 20 and 40 km (see Supplementary Table 5). In Fig. 3b, we also show the NSTF of the 1996 and 1960 tsunami earthquakes, the latter data coming from ref. 23.

**Rate-and-state model.** We model the time evolution of the westward displacement observed at GPS site BAYO using the rate-and-state formalism<sup>24</sup> and a one-dimensional spring-slider model. We use the analytical formulation proposed in ref. 26, which predicts the time evolution of slip for an area of velocity-strengthening submitted to a sudden stress increment induced by a co-seismic slip, modified by ourselves here for the case of two successive earthquakes. The estimated parameters of the model are a co-seismic offset after the 15 February earthquake, the velocity increment after each earthquake and a relaxation time. The wrms of the fit is 1.2 mm. Further details are provided in the Supplementary Information.

**Code availability.** The codes used for the GPS analysis and fault slip inversion are available on request from JMN.

## References

- Herring, T. A., King, R. W. & McClusky, S. C. *Documentation of the MIT GPS Analysis Software: GAMIT v 10.50*, Massachusetts Institute of Technology, (2013); <http://www-gpsg.mit.edu/~simon/gtgk>
- Hayes, G. P., Wald, D. J. & Johnson, R. L. Slab1.0: A three-dimensional model of global subduction zone geometries. *J. Geophys. Res.* **117**, B01302 (2012).
- Okada, Y. Internal deformation due to shear and tensile faults in a half-space. *Bull. Seismol. Soc. Am.* **82**, 1018–1040 (1992).
- Tarantola, A. *Inverse Problem Theory* (SIAM, 2005).
- Radiguet, M. *et al.* Slow slip events and strain accumulation in the Guerrero gap, Mexico. *J. Geophys. Res.* **117**, B04305 (2012).
- Kissling, E., Ellsworth, W. L., Eberhart-Phillips, D. & Kradolfer, U. Initial reference models in local earthquake tomography. *J. Geophys. Res.* **99**, 19635–19646 (1994).
- Vallée, M., Charléty, J., Ferreira, A. M. G., Delouis, B. & Vergoz, J. SCARDEC: A new technique for the rapid determination of seismic moment magnitude, focal mechanism and source time functions for large earthquakes using body-wave deconvolution. *Geophys. J. Int.* **184**, 338–358 (2011).